EFFECT OF ALUMINUM FLAKE ORIENTATION ON COATING APPEARANCE

Li-Piin Sung, Maria E. Nadal, Mary E. McKnight, Egon Marx, Raphael Dutruc
National Institute of Standards and Technology
Gaithersburg, MD 20899, USA
and
Brent Laurenti
Eckart America, Louisville, KY 40211, USA

Abstract

The orientation of platelet-like pigments in coatings is affected by the processing conditions resulting in appearance variations of the final product. A set of aluminum-flake pigmented coatings having different flake orientations was prepared using various spray conditions. The orientations of individual flakes were determined using laser scanning confocal microscopy and appearance properties of the coatings were determined from optical reflectance measurements. A Gaussian orientation distribution was then used as input to a ray scattering model to calculate the optical reflectance of these coatings. The flake orientation distributions and the measured optical reflectance as a function of scattering angle are presented and the latter is compared to the calculated reflectance.

Introduction

Metallic coatings are the most popular exterior finish in the automotive industry and are widely used on other products such as cellular phones and biking helmets. The changes in lightness with illumination and viewing angles draw attention to the geometric features of these items.[1-3] A metallic finish consists of metallic flakes, typically aluminum (Al) flakes, in a polymer binder, which is often pigmented to create different color appearance. Four key parameters can directly affect the optical properties of the metallic coatings: flake size, flake surface roughness, spatial orientation of the flakes, and other pigments (additives). This paper will mainly address the effect of the flake orientation on coating appearance. The flake orientation is strongly dependent upon the surface treatments of the flakes and the processing conditions.[1] Thus, it is crucial to be able to measure flake orientation accurately and to develop a methodology that can correlate flake orientation to the optical properties of the materials. The methodology will provide support for control and prediction of appearance for product design, manufacture, and marketing.

Many efforts have been made to investigate the interrelation between formulation, processing, and spatial distribution of Al flakes in surface coatings and their appearance properties. Only a few studies[4-7] have included quantitative measurements of the flake orientation in the cured coatings. Usu-

ally, the flake orientation was determined using microscopy techniques applied to sectioned, cross-cut samples. This approach does not address directly the three-dimensional (3D) spatial orientation of the flakes. Recently, Kettler and Richter[7] used combined techniques of goniospectrophotometry, confocal laser scanning microscopy, and microscopy image analysis of cross-cut samples to obtain 3D orientation information. However, the analysis of this approach was complex and the method was not direct. Furthermore, it is not obvious that one can deduce appearance properties directly from the orientation data described in their paper.

A long-standing issue is how to characterize the flake orientation accurately and how to correlate orientation information with the optical properties. To tackle these problems quantitatively, we have implemented a methodology to link the flake orientation data to the optical properties by integrating measurements and modeling efforts. In this paper, we describe the general approach for this methodology as follows: (1) determining 3D spatial orientation distribution of the normals to the flakes using non-destructive laser scanning confocal microscopy, (2) modeling the link between the flake orientation distribution and the optical properties of the coating using a ray scattering model and applying Gaussian flake orientation distributions of varying widths as input to the ray scattering model to calculate the optical reflectance, (3) measuring the angular distribution of the light scattered by the coating, and (4) comparing the measured results to the calculated optical reflectance from the model.

Experimental

(1) Materials

Two gray metallic pigmented coatings were prepared using a conventional hand-held spray gun. The coating was applied to a smooth black glass substrate without applying a top clearcoat. The coating consisted of an Al pigment in an acrylic-melamine polymer binder. The pigment was a special automotive grade that has a smooth surface finish and a disk-like shape. The pigment loading level was 5% by mass fraction based on solid content of the coating and the average flake size was about 16 μm. We changed the coating appearance using the same coating formula by varying the amount of fluid allowed to pass through the spray gun. The samples were designated according to the position of the fluid control as 1-turn and 1.5-turn for normal operation and extra fluid output, respectively. The final dry film thickness of samples was 38 μm ± 4 μm, measured by using a Positector 6000 series coating thickness gauge.[a]

Visually, all samples appeared lighter (greater brightness) near the specular direction and became darker as the viewing angle moved away from this direction. The brightness difference between these two samples was small but visually detectable, and in the range of the rejection criteria for metallic samples in an automotive processing line.

[a] Certain instruments or materials are identified in this paper in order to adequately specify experimental details. In no case does it imply endorsement by NIST or imply that it is necessarily the best product for the experimental procedure.

(2) Microstructure Characterization

We used a Zeiss model LSM510[a] laser scanning confocal microscope (LSCM) to characterize the microstructure of the coatings. A LSCM uses coherent incident light and collects reflected or scattered light exclusively from a single plane, rejecting light out of the focal plane. The wavelength, numerical aperture (N.A.) of the objective, and the size of the collecting pinhole in front of the detector determine the resolution in the thickness or axial direction.[8] In this study, an oil immersion objective (100×/1.3) was used. The scanning area of each confocal micrograph was about 92.1 μm × 92.1 μm at 0.18 μm/pixel, with a scanning time of 8 s/frame. The transverse and depth resolutions (point-to-point spread function) for an objective with a N.A. of 1.3 are 155 nm and 286 nm, respectively, for a scanning laser wavelength of 543 nm.

Figure 1a gives an example of a LSCM micrograph of an Al-pigmented coatings. All LSCM micrographs consist of images of overlapping optical slices (a stack of z-scan images) with a 0.3-μm z-step. The size and orientation of an individual flake can be extracted and calculated from the topographic data as illustrated in Figure 1b, and details will be discussed later in the theory section.

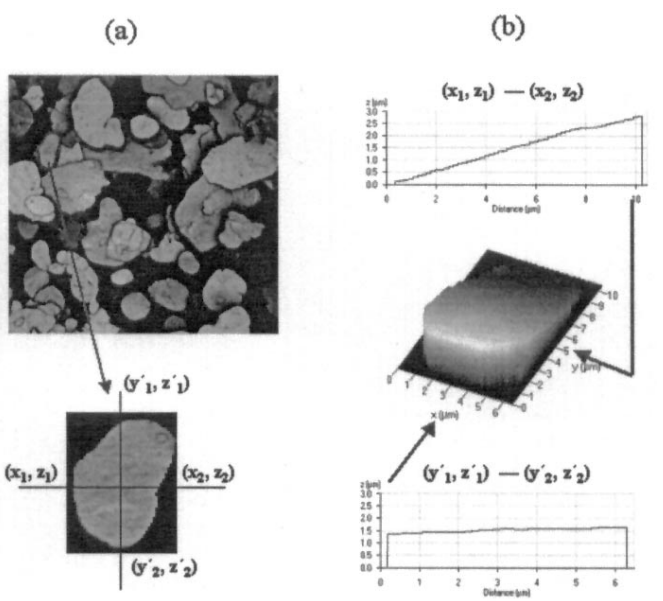

Figure 1: (a) LSCM image of intensity profile in a 2D projection and an extraction of an individual flake. (b) Definition of the size and orientation of an individual flake used in this paper.

(3) Optical Reflectance Measurement

The in-plane bi-directional reflectance for two metallic pigmented samples was measured using the NIST spectral tri-function automated reference reflectometer (STARR).[9] The incident light flux was a collimated, monochromatic, polarized beam with a diameter of 14 mm and a bandwidth of 15 nm for a wavelength of 550 nm. Two rotation stages determine the incident angle of the beam on the

sample and the viewing angle of the detector. Reflectance was calculated from the ratio of the reflected to the incident radiant flux. The incident flux was measured with the sample out of the beam path and the receiver positioned to accept the incident beam. The reflected radiant flux was measured with the sample in the beam path and the detector positioned at the desired geometry. Figure 2 presents the optical geometry, where θ_o and θ_s are angles of incidence and scattering measured with respect to the normal of the sample, and $\theta_s = -\theta_o$ is the specular reflection angle.

We measured the reflected intensity over a wide range of viewing angles for incident angles of 0°, 30°, 45°, 60°, and 75°, using unpolarized incident light at the wavelength of 550 nm. Viewing angles with respect to the normal to the surface of the sample ranged from –70° to + 70° at 0.5° increments. The expanded relative uncertainty for the reflectance data was 0.7 % (k = 2), calculated according to the procedures outlined in Ref. 9.

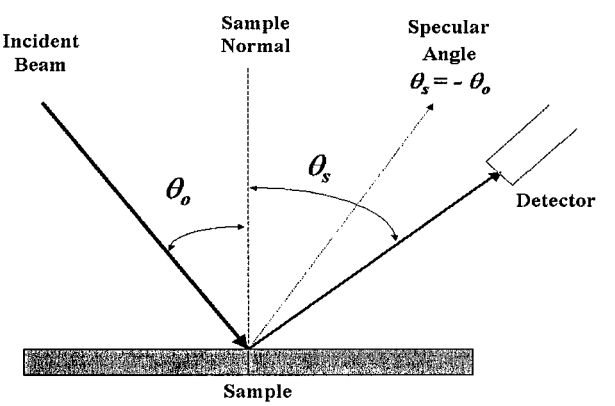

Figure 2: Optical geometry for the incident and scattering angles.

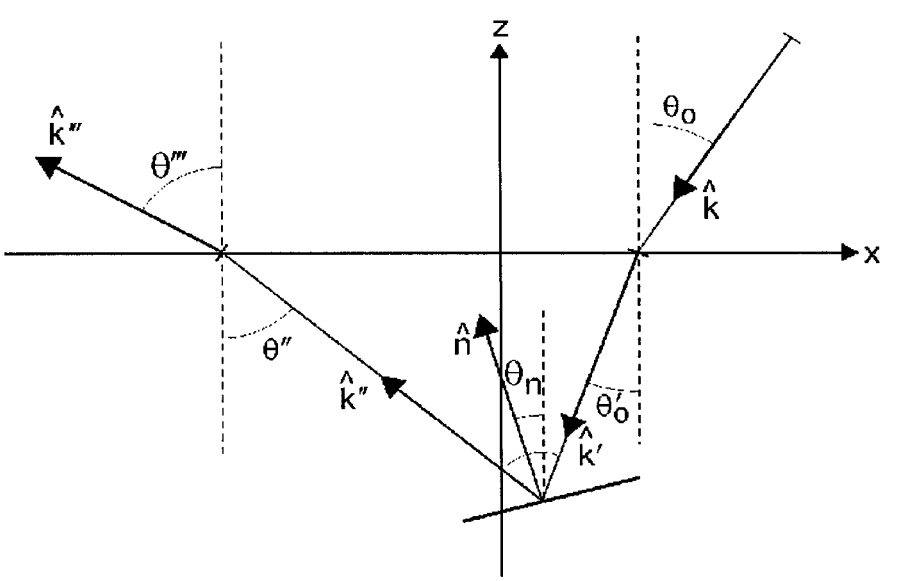

Figure 3: Ray trajectory for an oblique flake

Theory - Ray Scattering Model

The metallic flakes are significantly larger than the wavelength of light and tend to be oriented parallel to the coating surface. As a first approximation, we assume that the flakes are flat discs of perfectly conducting material and ignore multiple reflections. The angular distribution of the light scattered by the flakes can then approximately be determined from ray reflection by the flake surface. Roughness of the coating surface and flake surface also cause diffuse scattering. We first address the definition of the distribution of the angle between the normal of the flakes and the normal to the surface of the coating; then relate this distribution to the angular distribution of scattered light intensity.

(1) Distribution of the Normals to the Flakes

We chose a coordinate system with the *z*-axis perpendicular to the average plane of the surface, so that the normal to the surface is $\hat{e}_z$ and the *x*-axis is in the plane of incidence. We designate by $\hat{n}$ the unit normal to a flake. If $\hat{n}$ has spherical coordinates θ_n and φ_n we have

$$\hat{n} = n_x\hat{e}_x + n_y\hat{e}_y + n_z\hat{e}_z = \sin\theta_n \cos\varphi_n \hat{e}_x + \sin\theta_n \sin\varphi_n \hat{e}_y + \cos\theta_n \hat{e}_z \,. \tag{1}$$

We assume that the distribution of the orientation of the flakes is independent of the azimuthal angle and of the size of the flake. Since the intensity of the light scattered in a given direction is proportional to the total surface at a given angle, the determination of the distribution of the normal has to take into account the size of the flakes instead of just the number of flakes.

We call $p_2(\theta_n,\varphi_n)\mathrm{d}\Omega$ the probability that the spherical angles of the normal direction lie within a solid angle $\mathrm{d}\Omega$ about θ_n and φ_n. This probability distribution is assumed to be independent of φ_n. Then, if $p(\theta_n)\mathrm{d}\theta$ is the probability that the polar angle lies within an angle $\mathrm{d}\theta$ about θ_n, we have that

$$p(\theta_n)\mathrm{d}\theta = \int_0^{2\pi} p_2(\theta_n,\varphi)\sin\theta_n \mathrm{d}\varphi \mathrm{d}\theta = 2\pi\, p_2(\theta_n,0)\sin\theta_n \mathrm{d}\theta \,, \tag{2}$$

whence the two probability densities are related by

$$p(\theta_n) = 2\pi\, p_2(\theta_n,0)\sin\theta_n \,. \tag{3}$$

This is the function that we can determine from confocal microscopy measurements. We do not expect the function $p_2(\theta_n,\varphi_n)$ to diverge on the polar axis, so that we work with a modified distribution function

$$\tilde{p}(\theta_n) = p(\theta_n)/\sin\theta_n \tag{4}$$

and assume that the limit of the fraction is finite as $\theta_n \to 0$. We then have

$$p_2(\theta_n, \varphi_n) = p(\theta_n)/(2\pi \sin\theta_n) = \tilde{p}(\theta_n)/(2\pi). \tag{5}$$

A confocal microscope can determine the z-coordinate of the surface of a flake as a function of position, that is, $z(x, y)$ can be measured experimentally. If the surface is a plane, its equation has the form

$$\hat{n} \cdot \vec{x} = h \quad \Rightarrow \quad z = -(n_x/n_z)x - (n_y/n_z)y + h/n_z = ax + by + c. \tag{6}$$

The microscope can give the lines of constant x or of constant y; in particular, we can obtain the coordinates at the beginning and at the end of such a line. If they are (x_1, z_1) and (x_2, z_2) for a line of constant y, and (y_1', z_1') and (y_2', z_2') for a line of constant x, as shown in Figure 1b, the angle θ_n is given by

$$\tan^2\theta_n = \tan^2\theta_x + \tan^2\theta_y = \zeta_x^2 + \zeta_y^2 = \left(\frac{z_2 - z_1}{x_2 - x_1}\right)^2 + \left(\frac{z_2' - z_1'}{y_2' - y_1'}\right)^2. \tag{7}$$

An estimate of the area of the flake can be obtained from

$$S \propto (x_2 - x_1)(y_2' - y_1')/(\cos\theta_x \cos\theta_y). \tag{8}$$

We thus find the distribution of the flake orientation by computing θ_n from Eq. (7) and adding a contribution equal to the area in Eq. (8) to the corresponding bin.

Barrick[10] has addressed a related problem — the connection between the angular distribution of scattered light and the slope and curvature distributions of a rough surface. He defines a probability density that we designate by $P_2(\zeta_x, \zeta_y)$, ignoring the dependence on higher-order derivatives. If the surface is isotropic, P_2 depends only on $\zeta = \tan\theta_n = (\zeta_x^2 + \zeta_y^2)^{1/2}$. We relate the distribution $P(\zeta) = 2\pi\zeta P_2(\zeta_x, \zeta_y)$ to ours and find

$$\tilde{p}(\theta_n) = P(\tan\theta_n)/(\sin\theta_n \cos^2\theta_n). \tag{9}$$

(2) Determination of the Path Followed by a Ray

We now determine the path followed by the incident ray as it is refracted at the surface of the coating, then reflected by a metallic flake, and then refracted again as it exits the coating, as shown in Figure 3. If the instrument is restricted to take measurements in the plane of incidence and if we neglect the effect of the aperture, we can ignore the dependence on the azimuthal angle φ.

The incident beam comes in along the xz-plane in the direction defined by the angle θ_0; the azimuthal angle φ_0 vanishes. This beam is refracted into the coating where it propagates in the direction $\hat{k}'$ at an angle θ_0'. We designate by n the real index of refraction of the coating. Then the angle

θ_0' is determined by Snell's law, that is, $n \sin\theta_0' = \sin\theta_0$. The intensity of the refracted beam is determined by the Fresnel coefficients, which in turn depend on the polarization of the incident field. The angular dependence of the coefficients, as well as their dependence on polarization, is assumed to be negligible. If only the intensity of the outgoing beam relative to that in the specular direction is used in the analysis, such constants can be ignored.

The ray is then specularly reflected by the flake in the direction $\hat{k}''$, assuming that Al flakes are perfect conductors, and refracted again at the boundary of the coating in the direction $\hat{k}'''$. If we restrict ourselves to the plane of incidence, the corresponding angles of the propagation vectors are related again by Snell's law, which in this case implies that $\sin\theta''' = n \sin\theta''$. The refracted ray is not necessarily in the plane of incidence and the azimuthal angles satisfy $\varphi''' = \varphi'' = \varphi$. Then from geometric consideration, the angle that the normal to the flake makes with the z-axis is

$$\hat{n} = (\hat{k}'' - \hat{k}') \Big/ \left| \hat{k}'' - \hat{k}' \right|, \tag{10}$$

which determines θ_n and φ_n.

The factor γ that determines the projection of the area perpendicular to the beam incident to the flake is the cosine of the angle between the normal to the flake and the direction of the incident beam in the substrate, that is,

$$\gamma(\theta_n, \varphi_n, \theta_0) = -\hat{n} \cdot \hat{k}' = (1 - \hat{k}'' \cdot \hat{k}')(2 - 2\hat{k}'' \cdot \hat{k}')^{-1/2} = [(1 - \hat{k}' \cdot \hat{k}'')/2]^{1/2}. \tag{11}$$

The normal as a function of the variables of integration $\bar{\theta}$ and $\bar{\varphi}$ in a new coordinate system where the z-axis coincides with the axis of the jth detector is given by

$$\theta_n = \Theta_j(\bar{\theta}, \bar{\varphi}; \theta_0), \quad \varphi_n = \Phi_j(\bar{\theta}, \bar{\varphi}; \theta_o). \tag{12}$$

The functions depend on θ_0 because which flake reflects the incoming ray into the given direction in the detector depends on the angle of incidence. The angle θ_n of the normal to a flake that reflects a ray incident at an angle θ_0 is given by

$$\sin\theta_n = \left[\frac{\sin^2\theta'' + 2\sin\theta''\cos\varphi\sin\theta_0' + \sin^2\theta_0'}{2 + 2(\sin\theta''\cos\varphi\sin\theta_0' + \cos\theta''\cos\theta_0')} \right]^{1/2}. \tag{13}$$

(3) Light Scattering Distribution

To connect a distribution of the normals to the flakes to measurements made with an instrument we integrate over the angular aperture of a detector, given by the half-angle α. We assume that the jth detector, or the jth position of a single detector, is located in a direction given by the spherical coordinates ϑ_j and φ_j, $j = 1, \ldots, N$.

If all the light reflected by the metallic flakes in a particular direction is collected by the detector in that direction, the intensity of the light scattered is proportional to the probability that at the normal to the flake be oriented so that the light is reflected into the detector from the incident beam. The part of the incident beam that is reflected by a flake is then proportional to total flake area projected perpendicular to the beam. To obtain the intensity, up to a factor, of the light scattered into the jth detector we have to integrate the probability distribution over the detector aperture $\Delta\Omega$,

$$\begin{aligned} I_j(\theta_0) &= \int_{\Delta\Omega(\vartheta_j,\varphi_j)} \mathrm{d}\Omega''' \gamma(\theta_n,\varphi_n,\theta_0) p_2[\theta_n(\hat{k}''',\theta_0),\varphi_n(\hat{k}''',\theta_0)] \\ &= [1/(2\pi\sqrt{2})] \int_{\Delta\Omega(\vartheta_j,\varphi_j)} \sin\theta'''\,\mathrm{d}\theta'''\,\mathrm{d}\varphi (1-\hat{k}'\cdot\hat{k}'')^{1/2}\,\tilde{p}[\theta_n(\hat{k}''',\theta_0)]. \end{aligned} \tag{14}$$

Note that $\hat{k}'$ is determined by θ_0 and $\hat{k}''$ by $\hat{k}'''$.

This integral can be rewritten in the new coordinate system. The integral in Eq. (14) then reduces to

$$I_j(\theta_0) = (1/2\pi)\int_0^{\alpha} \sin\bar{\theta}\,\mathrm{d}\bar{\theta} \int_0^{2\pi} \mathrm{d}\bar{\varphi}\gamma(\theta_n,\varphi_n,\theta_0)\tilde{p}[\Theta_j(\bar{\theta},\bar{\varphi};\theta_0)], \tag{15}$$

where the angle of the normal to the flake with the normal to the surface is given by a function Θ_j for each detector, as stated in Eq. (12).

We assume that $p(0)=0$ and that $\tilde{p}(0)$ is finite. If the integrand varies significantly over the region of integration, the integral in Eq. (15) is best evaluated numerically. A spherical cap of angle θ_c is defined around the axis of the detector and its contribution is computed separately, whence

$$\begin{aligned} I_j(\theta_0) &\approx (\theta_c^2/4\pi)\gamma(0,0,\theta_0)\tilde{p}[\Theta(0,0;\theta_0)] \\ &\quad + (\Delta\bar{\theta}\Delta\bar{\varphi}/2\pi)\sum_{i=1}^{N_\theta}\sin\bar{\theta}_i \sum_{i'=1}^{N_\varphi}\gamma(\bar{\theta}_i,\bar{\varphi}_{i'},\theta_0)\tilde{p}[\Theta_j(\bar{\theta}_i,\bar{\varphi}_{i'};\theta_0)], \end{aligned} \tag{16}$$

where,

$$\Delta\bar{\theta} = (\alpha-\theta_c)/N_0, \quad \bar{\theta}_i = \theta_c + (i-\tfrac{1}{2})\Delta\bar{\theta}, \quad \Delta\bar{\varphi} = 2\pi/N_\varphi, \quad \bar{\varphi}_i = (i'-\tfrac{1}{2})\Delta\bar{\varphi}. \tag{17}$$

The value of $\bar{\varphi}$ is of course undefined when $\bar{\theta}$ vanishes even though we have assigned the value 0 to it.

If the functions γ and $\tilde{p}$ in Eq. (15) are approximately constant across the solid angle, which probably is a good approximation when the specular direction is not within or near the detector, we have

$$\begin{aligned} I_j(\theta_0) &\approx \gamma(0,0,\theta_0)\tilde{p}[\Theta_j(0,0;\theta_0)]/(2\pi)\int_0^{\alpha}\sin\bar{\theta}\,\mathrm{d}\bar{\theta}\int_0^{2\pi}\mathrm{d}\bar{\varphi} \\ &= (1-\cos\alpha)[(1+\sin\theta_0'\sin\vartheta_j'\cos\varphi_j+\cos\theta_0'\cos\vartheta_j')/2]^{1/2}\,\tilde{p}[\Theta_j(0,0;\theta_0)]. \end{aligned} \tag{18}$$

For small α, I_j is proportional to α^2, that is,

$$I_j(\theta_0) \approx \tfrac{1}{2}\alpha^2[(1+\sin\theta_0'\sin\vartheta_j'\cos\varphi_j+\cos\theta_0'\cos\vartheta_j')/2]^{1/2}\,\tilde{p}[\Theta_j(0,0;\theta_0)]. \tag{19}$$

Results and Discussion

The LSCM technique provides a non-destructive, powerful tool for characterizing the Al flakes in the coatings. Figure 4 shows the LSCM images of samples prepared under different spray conditions. The upper set of images represents the intensity profile in 2D projection and the lower set of images represents the topographic profile of the Al flakes distribution in a series of z-scan optical slices. The dark areas indicate the absence of Al flakes in the probed region. The shapes of the flakes appear to be platelet-like and surfaces of individual flakes are reasonably smooth. Slight variations in the sizes and shapes of flakes can also result in differences in appearance due to different spatial distributions of normals.[2]

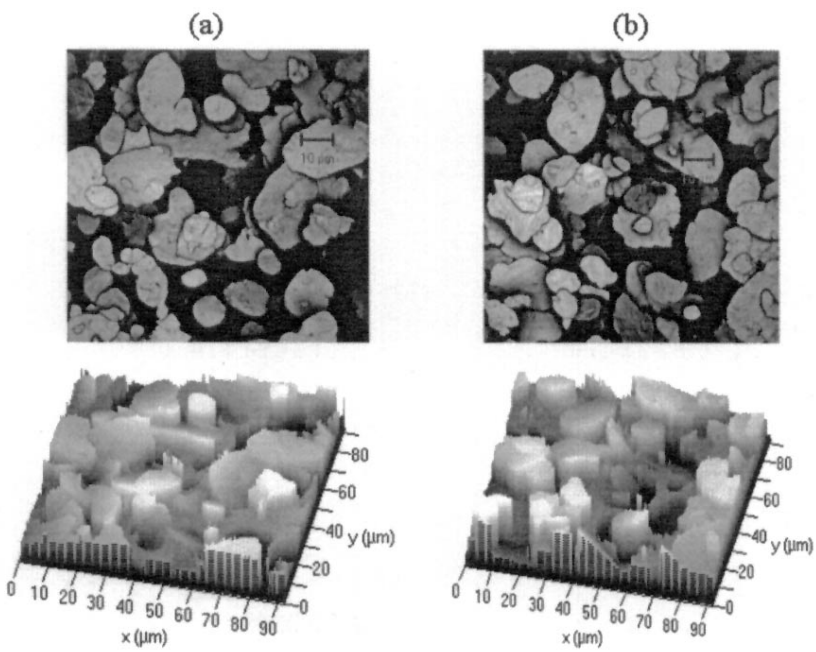

Figure 4: LSCM images for two metallic pigmented samples (a) 1-turn and (b) 1.5-turn in 2D intensity projection (upper) and topographic (bottom) presentations.

To obtain good statistics for characterizing the spatial distribution of flakes, we used 6 to 10 micrographs (410 flakes for 1-turn sample and 310 flakes for 1.5-turn sample in total). Figure 5a shows the orientation (or inclination) distribution of the flakes in the 1-turn sample in terms of θ_x and θ_y, using the definition in the theory section and illustrated in Figure 1b. We used Eq. (7) to calculate the surface normal angle, θ_n, and the resulting distribution function is shown in Figure 5b. As mentioned previously, the intensity of the light scattered in a given direction is proportional to the total surface at a given angle. Thus, the determination of the distribution of the normals needs to take into account the size of the flakes rather than the number of flakes. Figure 5c shows the flake distribution, $p(\theta_n)$, after taking into account the flake area using Eq. (8). Note that all histograms in Figure 5 were results obtained from 410 flakes of the 1-turn sample and the data are sorted by 1° per bin.

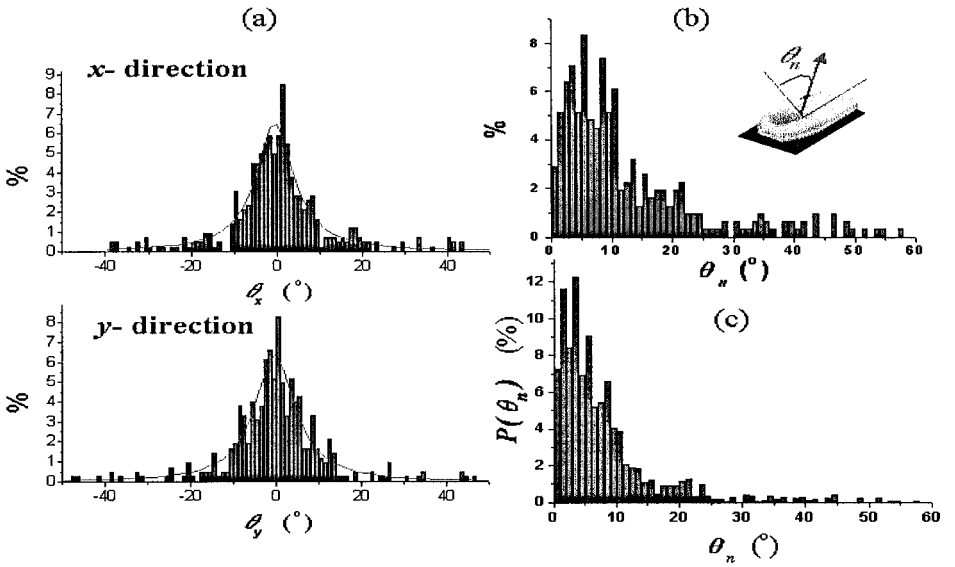

Figure 5: Histograms for the 1-turn sample: (a) angular distribution of the orientations in the x- and y-directions, θ_x, θ_y, (b) distribution of the flake normal angle, θ_n, and (c) flake orientation distribution function $p(\theta_n)$.

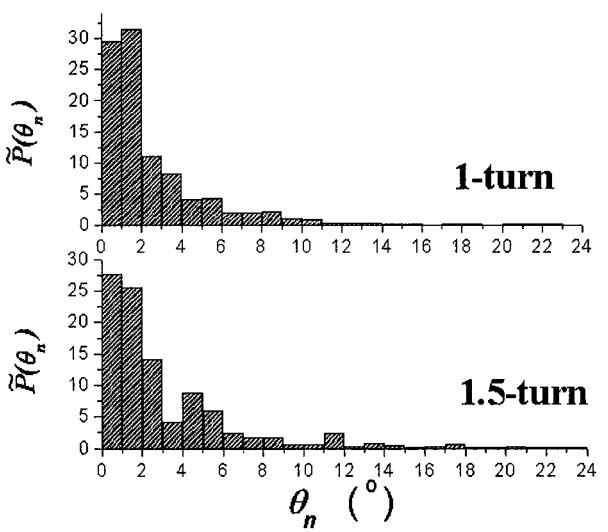

Figure 6: Histograms of the modified flake orientation distribution functions, $\tilde{p}(\theta_n)$, for 1-turn and 1.5-turn samples.

We then calculated the modified orientation distribution of flakes, $\tilde{p}(\theta_n)$, using Eq. (4). Figure 6 shows $\tilde{p}(\theta_n)$ for both 1-turn and 1.5-turn samples. The distributions do not appear to have a well-defined shape and are "noisy," especially for the 1.5-turn sample. Additional, ongoing data collection should produce better statistics.

Figure 7 shows the calculated intensity distribution (reflectance normalized to 1 in the specular direction) at two incident angles as a function of scattering angle for two Gaussian modified angle distribution functions, $\tilde{p}(\theta_n)$, with half-widths $w = 4°$ (close to the estimated half-width of $\tilde{p}(\theta_n)$ obtained for 1-turn sample in Figure 6) and $w = 10°$ using Eq. (16). It is obvious from the geometry in Figure 3 that the intensity distribution will be wider than the angle distribution, and that the index of refraction, which for the coatings is approximately 1.5, will also contribute to this widening. The graphs in Figure 7 for $w = 10°$ illustrate the fact that the maximum reflectivity is not in the specular direction.

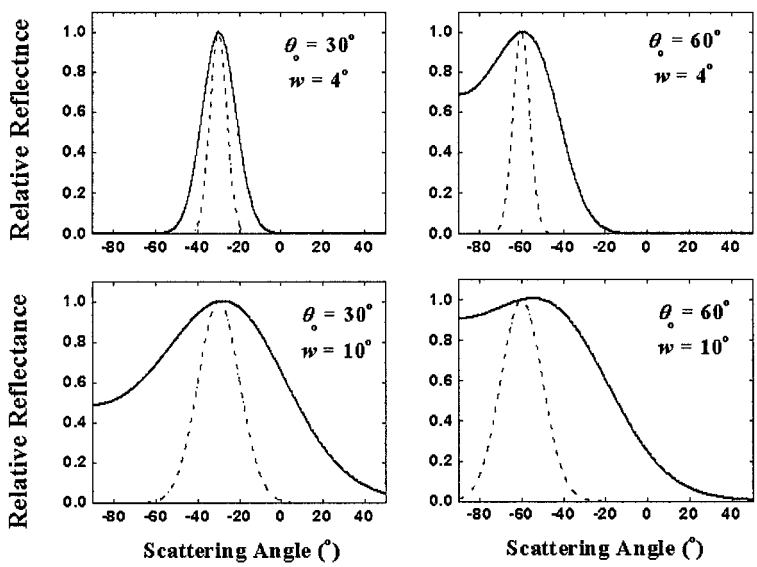

Figure 7: Calculated relative reflectance as a function of scattering angle. Solid lines: calculated normalized reflectance. Dashed lines: Gaussian flake orientation angular distribution functions centered at 0° with a half-width w, plotted about the specular direction.

Figure 8 shows the reflectance data for incident angles of 30° and 60° for the two samples. The results at other incident angles are similar in shape. We verified the isotropy of the samples by measuring the gonio-distribution of the reflectance for several position of the sample as it was rotated about the normal of the surface. The measurements indicated that the samples were isotropic over the 14 mm diameter illuminated region. The reflectance data are very similar in the specular region (between two dashed lines) since both samples contained the same polymer binder. Furthermore, comparisons with the angular distribution of the light scattered by smooth epoxy coatings[11] and by coatings containing a thick layer of a top clearcoat suggested that the measured intensity in the specular region (half-width ≈ 1.5°) corresponds to the reflection by the top surface of the coating and not to the scattering by the flakes. In addition, we were able to confirm this hypothesis by a polarization scattering technique and distinguish different scattering sources and mechanisms of the scattered intensity.[12] The underlying "off-specular" (few degrees away from the specular peak) reflectance is due to scattering from the subsurface microstructure — mostly from the reflections from the flakes.

Because additional planned experiments that will allow us to separate the scattering contribution from the top surface have not been completed, we estimated the half-width of intensity angular distribution from measured reflectance data. The 1.5-turn sample has a relatively larger "off-specular" intensity but a somewhat narrower half-width angle of ~11°, while the half-width angle of 1-turn sample is ~14°.

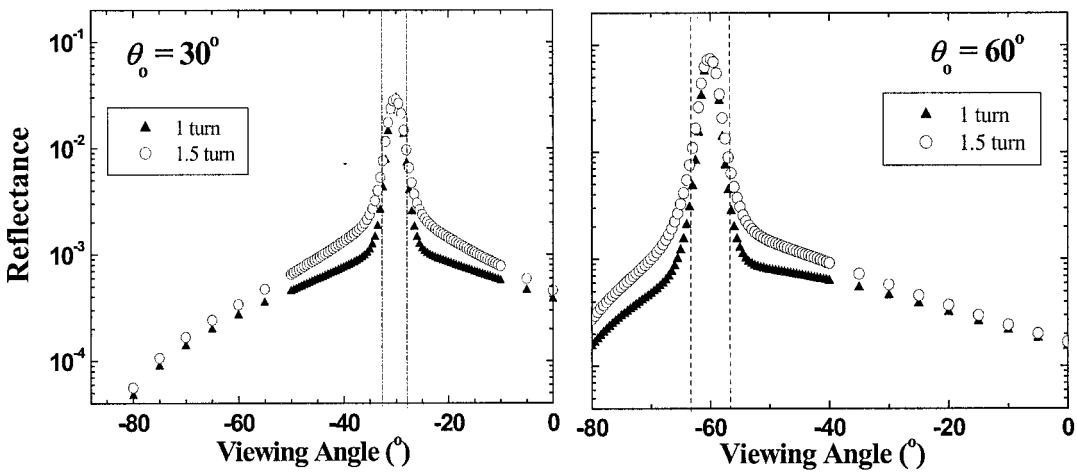

Figure 8: Measured optical reflectance data as a function of viewing angles at two angles of incidence for two metallic samples.

Figure 9 shows the comparison between the measured reflectance data and the calculated reflectance using a Gaussian modified angle distribution of flakes, $\tilde{p}(\theta_n)$ with half-width $w = 6°$, which provides a reasonable fit to the data. The data match quite well near the specular region (excluding the specular peak) and the discrepancy becomes larger as the viewing angle moves away from specular angles. Furthermore, the w value is greater than the estimated half-angle of 4° from the measured modified orientation distribution in Figure 6 for the 1-turn sample. This implies that the flake orientation (inclination) distribution is not the only scattering contribution. Factors that may contribute to this discrepancy were ignored in the simple ray scattering model. They include (1) contribution from top surface scattering near the specular region, (2) scattering from the local roughness of the flake surface, the edge of the flakes, and the overlapped flake clusters, (3) incorrect shape and half-width of distribution function, and (4) multiple-scattering. To address the issues mentioned above and to improve the current methodology used to link optical properties to microstructure data, we are continuing with the following work:

(1) Remove the contribution from top surface scattering near the specular region by applying a smooth layer of top clearcoat on top of the samples.
(2) Modify the ray scattering model to take into account the local surface roughness.
(3) Collect additional flake orientation data to obtain better statistics for determining a flake orientation distribution.

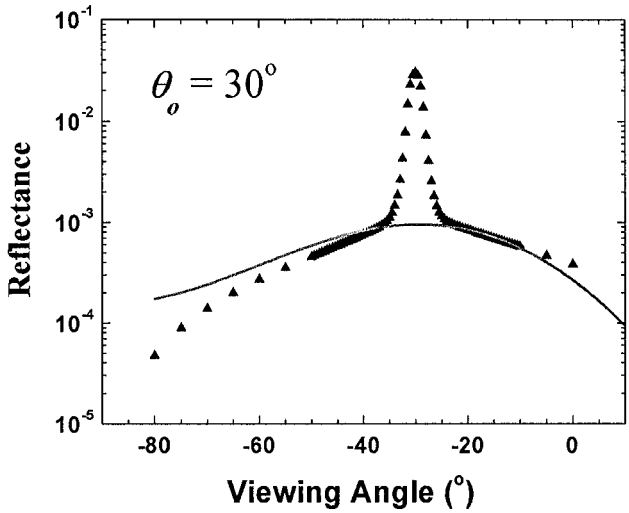

Figure 9: Comparison between measured (triangles) and calculated (solid line) reflectance of 1-turn sample using flake orientation angular distribution with Gaussian half-width angle of $w = 6^o$.

Acknowledgements

The authors would like to thank Dr. Thomas A. Germer for helpful discussion and polarization measurements and Michelle Clarke for helping in microstructure characterization. This research is part of the Measurement Science for Optical Reflectance and Scattering Project at NIST.

References

(1) Wicks, Z.W., Jones, F.N. Jr., Pappas, S.P., *Organic Coatings: Science and Technology*, John Wiley & Sons, Inc. (1992).

(2) McCamy, C.S., "Observation and Measurement of the Appearance of Metallic Materials, Part I. Macro Appearance & Part II. Micro Appearance" *Color Research and Application*, **21**, 292-304 (1996), **23**, 362-372(1998).

(3) Rodrigues, A.B.J., "Color and Appearance Measurement of Metallic and Pearlescent Finishes," *ASTM Standardization News*, 68-72, October (1995).

(4) Tachi, K., Okuda, C., Suzuki, S., "Mechanism of Aluminum Flake Orientation in Metallic Topcoats," *Journal of Coatings Technology*, **62**, 43-50 (1990).

(5) Tachi, K., Okuda, C., "Color Variation of Automotive metallic Finishes," *Journal of Coatings Technology,* **64**, 71-77 (1990).

(6) Wojtkowiak, J.J., "Effect of Film Viscosity on Aluminum Flake Orientation in Thermoplastic Acrylic Coatings," *Journal of Coatings Technology*, **51**, 111-116 (1979).

(7) Kettler, W.H., Richter, G., "Investigation on Topology of Platelet-Like Effect-Pigments in Automotive Surface-Coatings," *Progress in Organic Coatings*, **31**, 297-306 (1997).

(8) Corle, T.R., and Kino, G.S., *Confocal Scanning Optical Microscopy and Related Imaging Systems*, Academic Press (1996).
(9) Barnes, P.Y., Early, E.A., Parr, A.C., *Spectral Reflectance*, NIST Special Publication, 250-48 (1998).
(10) Barrick, D.E., "Rough Surface Scattering Based on the Specular Point Theory," *IEEE Trans. Antennas Propagat.* **16**, 449-454 (1968).
(11) McKnight, M.E., Marx, E., Nadal, M.E., Vorburger, T.V., Barnes, P.Y., Galler, M., "Measurements and Predictions of Light Scattering by Clear Epoxy Coatings," *Applied Optics*, **40**, 2159-2168 (2001).
(12) Germer, T.A., and Asmail, C.C., "Polarization of light scattered by microrough surfaces and subsurface defects," *J. Opt. Soc. Am. A*, **16**, 1326-1332 (1999).